

4.3 ID Power

4.3.1 Overview

4.3.1.1 Subsystem Requirements and Overview (LY)

Table 4.3.1: Power Subsystem Requirements from 16.83

ID	Description	Parent	Verification
D.1	The power system shall supply power to each component within their current and voltage operating ranges.	A.5, A.12, A.13	Inspection Analysis
D.2	The power system shall monitor its health continuously.	A.13	Inspection

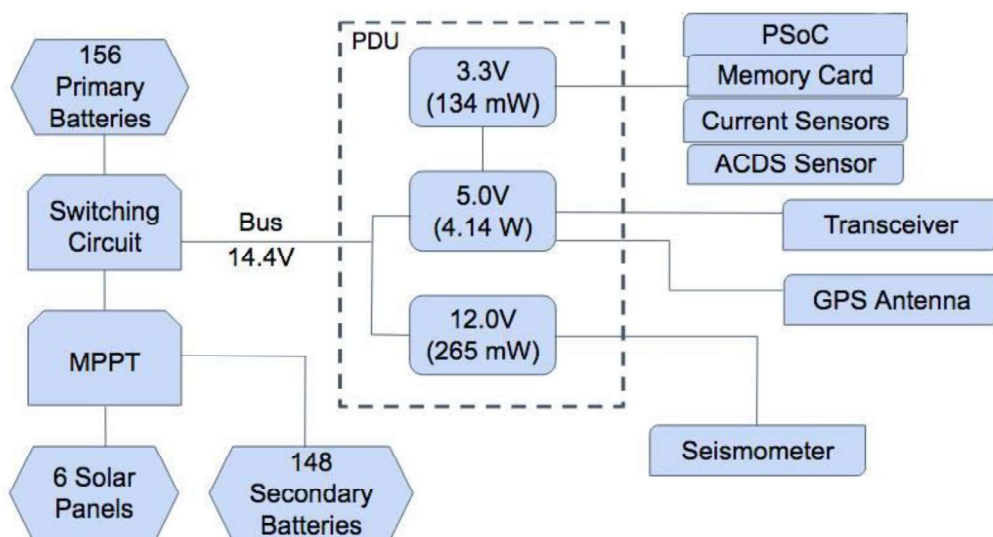


Figure 4.3.1: Block Diagram of Subsystem [CT]

As shown in Table 4.3.1, the first requirement for the Power subsystem is to power the electronics mentioned in the previous Avionics section and other instruments that will be mentioned in later sections. To do this, the Power subsystem is comprised of the components shown in Figure 4.3.1. The solar panels and secondary batteries are connected into the Maximum Power Point Tracker (MPPT) which takes input from the solar panels to charges the secondaries. When the secondaries are sufficiently charged, the MPPT discharges the secondaries into the switching circuit. When there is not enough voltage coming from the secondaries, the primary batteries will supply power. The

switching circuit is connected to the Power Distribution Circuit (PDU) which distributes and steps down the voltage so that other subsystems' components can be powered at the proper voltage.

The second requirement is to monitor the health of the power system continuously. To do this, there are current sensors on the Avionics Integration Board. However, due to time constraints, the Power and Avionics subsystems were not able to implement health monitoring.

4.3.1.2 Subsystem Cost (LY, JV)

In 16.831, the total cost of all of the parts ordered was \$3512.93. See [Appendix](#) for an itemized list of the purchases made. The current cost estimate of the proposed design for the final penetrator is (See Table 4.3.2 for a cost breakdown). This value has increased from 16.83 since the cost of printed circuit boards for the PDU, switching circuit, and wiring for the batteries were not accounted for. The fabrication costs associated with the aluminum casing for the solar panels were not accounted for either.

Table 4.3.2 Power Subsystem Proposed Budget for Final Mission [LY, JV]

Proposed Budget for Final Mission	
Component	Cost
156 OmniCel ER34615 3.6V 19Ah Li Batteries	\$1560
148 Panasonic 18650B 3.7V 3400mAh Rechargeable Li Batteries	\$940
Switching Circuit PCB with Components	\$80
Power Distribution Unit PCB with Components	\$165
2 Primaries Wiring PCB with Battery Contacts	\$100
Top Secondaries Wiring PCB with Battery Contacts	\$330
Bottom Secondaries Wiring PCB with Battery Contacts	\$330
Genesun MPPT	\$109
6 Triple Junction Solar Panels	\$27,500
Total	\$31,114

4.3.2 Individual Components

4.3.2.1 Primary Batteries Acceptance Testing (LY and EL)

In 16.83, OmniCel ER34615 D-Size 3.6V 19Ah Lithium batteries were chosen because of their high energy density. This section discusses the tests completed in order to verify the batteries' performance, in terms of low temperatures and long durations.

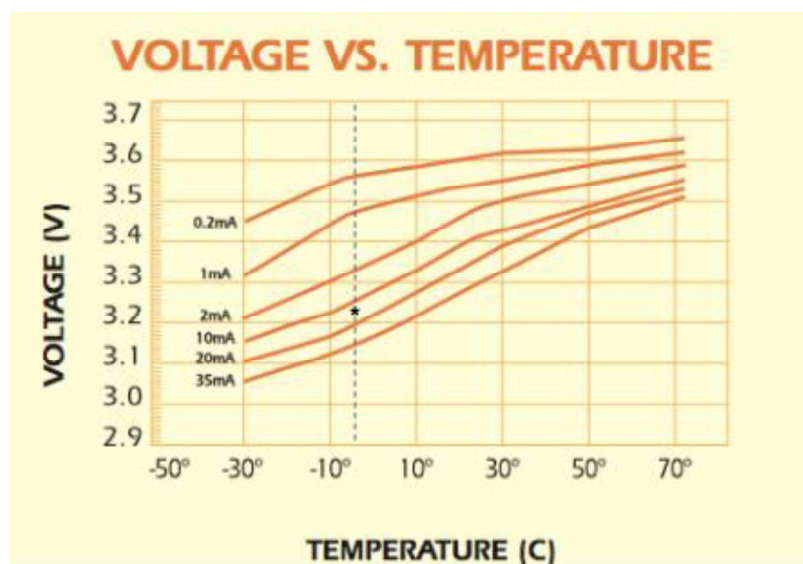


Figure 4.3.2: Primary Batteries Manufacturer's Specifications
in Various Temperatures

In the Freezer test, it is desired to demonstrate the ability of the primary batteries to perform by the manufacturer's specifications in low temperatures. The freezer was adjusted to 0°C, as this was the thermodynamics team's estimate of the interior of the penetrator. Two individual primary batteries and a thermocouple were placed inside the freezer. Wires connected the batteries to a breadboard with a 273 ohms resistor to produce a current of 0.013179 amps. This simulates the load the batteries will experience during the Dark Period. A volt logger was used to measure and record the volt for a duration of two hours. For a more detailed test plan, refer to Appendix I. Figures 4.3.3 and 4.3.4 show the results.

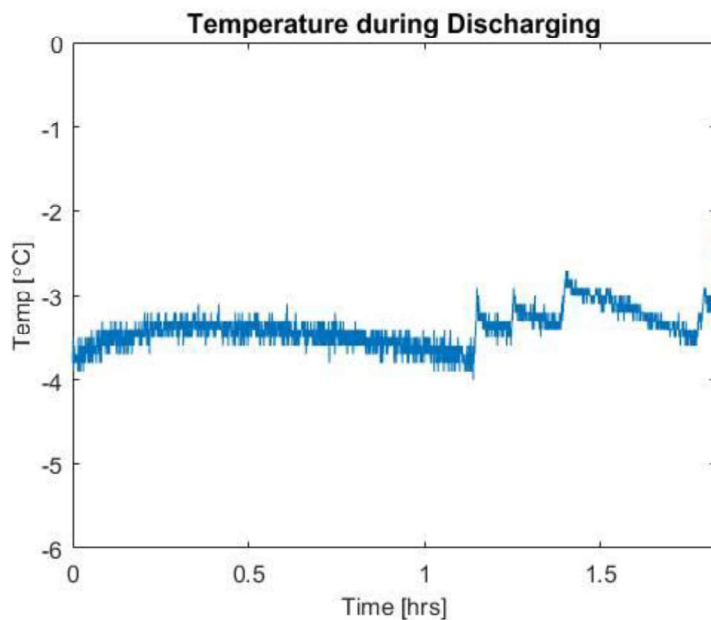


Figure 4.3.3: Temperature During Primaries Freezer Test [EL]

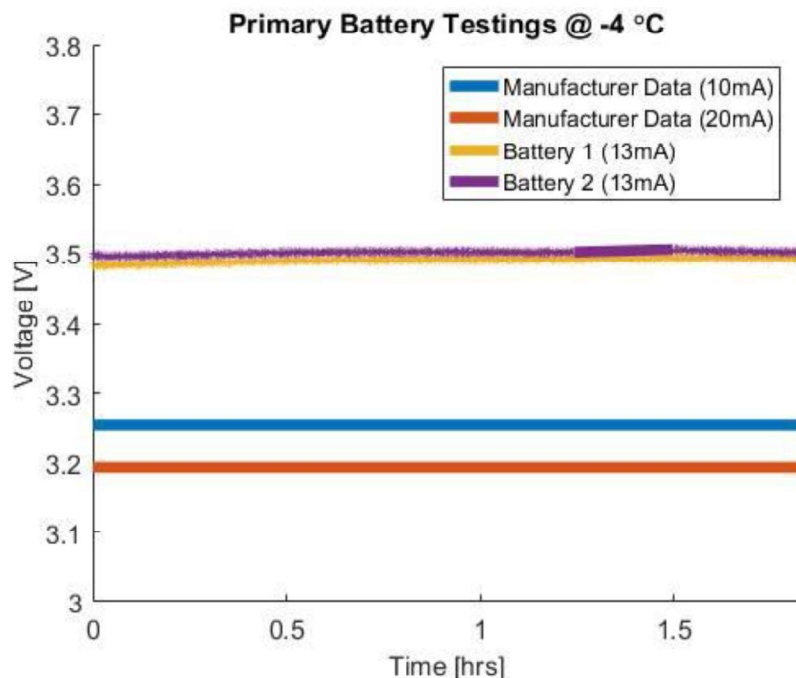


Figure 4.3.4: Voltage of Primaries During Freezer Test [EL]

As shown in Figure 4.3.3, the temperature inside the freezer was approximately -4°C. (It should be noted that the jumps in the temperature data was caused by opening the freezer.) From the manufacturer's specifications, at -4°C and 13 mA, the batteries should be discharging between 3.2 to 3.25 V, as indicated by the star in Figure 4.3.2. Thus, the success criteria of this test was that the batteries have to

be discharging at least 3.25 V to pass this acceptance test. As shown in Figure 4.3.4, the batteries discharged at roughly 3.5V; therefore, the primary batteries passed this test.

The Long Duration Test's purpose was to verify the primaries' discharge characteristics over a long duration of time. Ideally, the batteries would have been tested with the same load as they would experience during the Dark Period. However, this would have taken about 180 days to test, which is not feasible to do in a semester. Instead, it was decided to verify the manufacturer's specifications on the primaries' discharge characteristics.

The curve indicated by the red arrow in Figure 4.3.5 was chosen to be reproduced in order to have the quickest test. In a room with a temperature of 25°C, batteries were connected to a 60 ohm resistor via a breadboard to produce a current of 60 mA. A volt logger was used to measure and record the batteries' voltage for roughly 8 days. For a more detailed test procedure, refer to Appendix I.

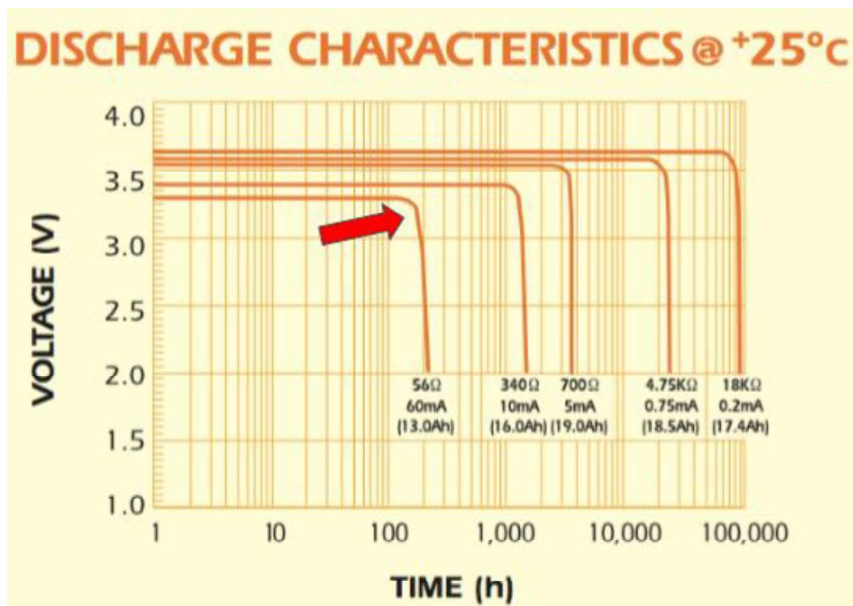


Figure 4.3.5: Primary Batteries Manufacturer's Specifications of Discharge Characteristics

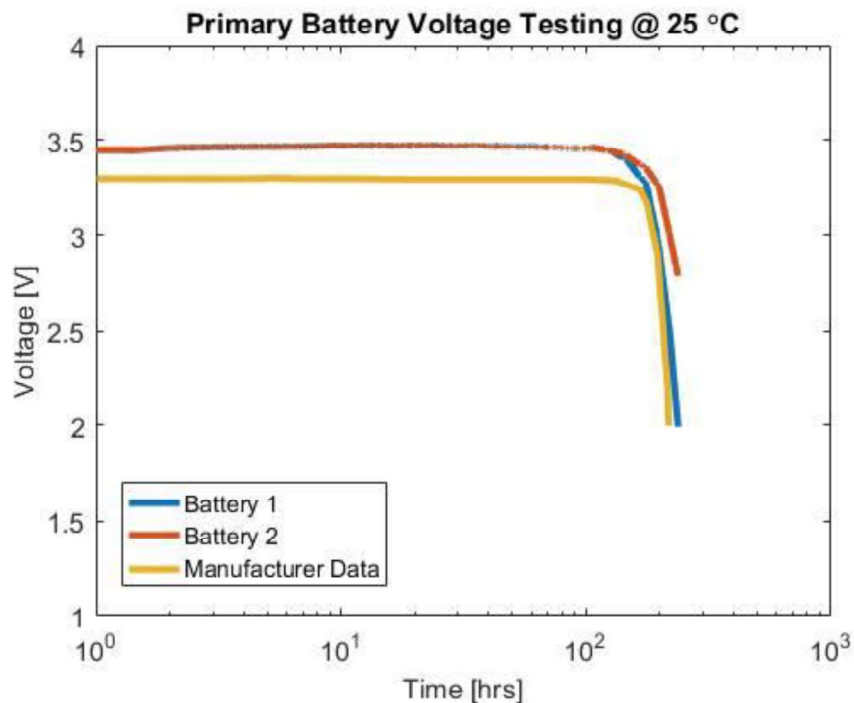


Figure 4.3.6: Primaries Voltage During Long Duration Test [EL]

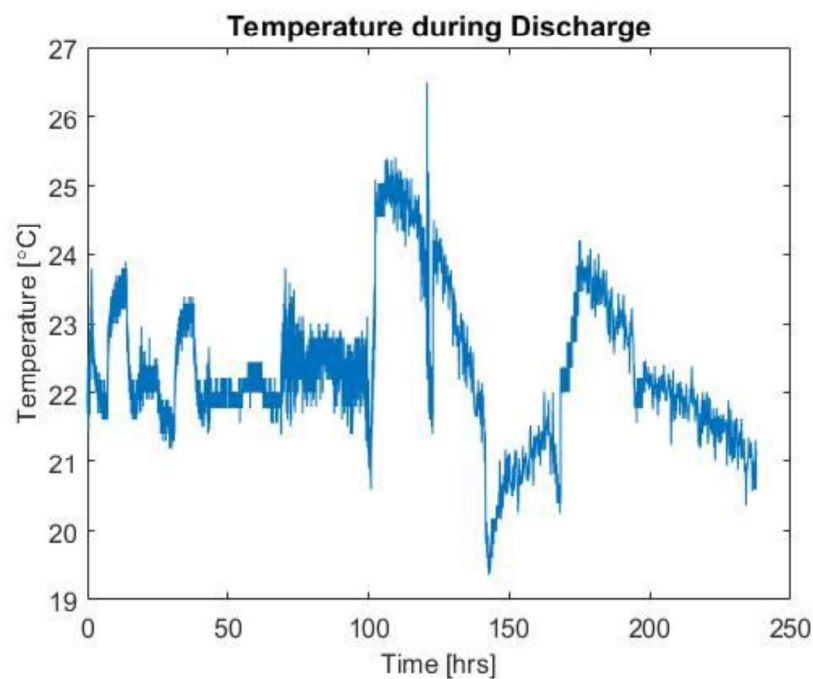


Figure 4.3.7: Temperature During Long Duration Test [EL]

In the final penetrator, 12V, the highest voltage requirement, needs to be supplied to the seismometer. Since the primaries are connected in series of four, the voltage of the primaries need to maintain above 3V. From the manufacturer's specifications, while pulling 60 mA at 25°C, the batteries drop to 3V at 186

hours. Thus, it is desired to show, and therefore the success criteria of this acceptance test, that the batteries drop to 3V after 186 hours. As shown in Figure 4.3.6, the voltage plots of the batteries are above and to the right of the manufacturer's specifications. This means that the batteries are supplying a higher voltage for a longer time. Thus, the batteries are performing better than the specifications. In particular, batteries 1 and 2 fall to 3V at 190 hours and 205 hours, respectively. Therefore, the primary batteries have passed their second acceptance test.

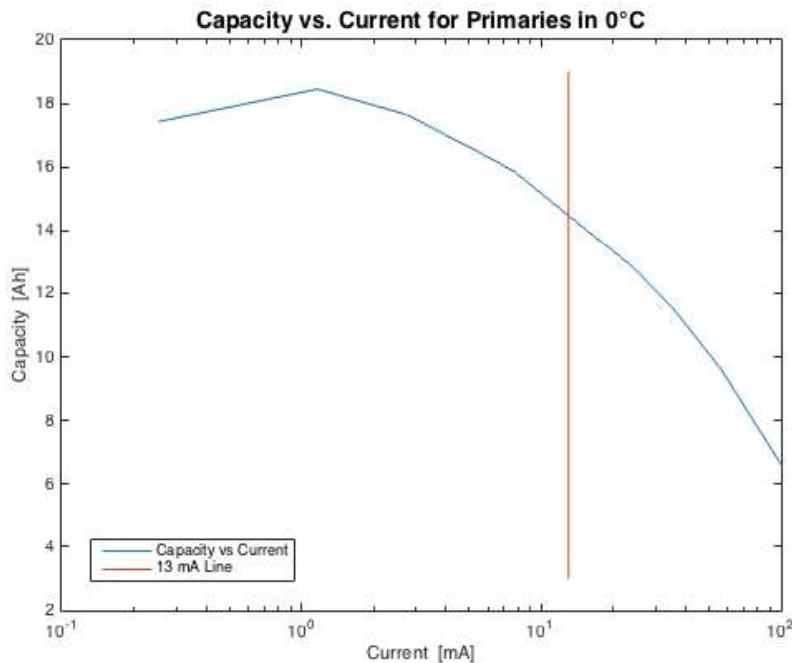


Figure 4.3.8 Specifications on Capacity vs. Current for Primaries in 0°C [LY]

By successfully passing the Freezer Test and the Long Duration Test, the battery's specifications have been verified. Therefore, the manufacturer's specifications can be trusted. During the Dark Period, each primary battery will push 13mA in 0°C. With these conditions, as shown in Figure 4.3.8, the expected capacity for a battery is 14.4 Ah. For the safety of the batteries, the depth of discharge will be 90%. With 156 primary batteries and an expected power consumption of 1.88W, the primary batteries are expected to last 161 days during the Dark Period. Although 161 days is less than 180 days, it should be noted that the pure dark period is only 116 days and has two transition periods, 34 days before and 30 days after the pure dark period. Thorough testing needs to be completed on the secondary batteries to see if both the secondaries and what is left of the primary batteries will sufficiently power the penetrator during the transition periods.

4.3.2.2 Printed Circuit Boards for Wiring Primary Batteries (LY and EL)

A stack of batteries consist of 52 batteries that are organized into 13 columns of 4 stacked batteries to connect them in series. In a stack, PCB's were designed to greatly reduce the amount of wiring needed to connect the columns in parallel. The Top PCB connects to the positive ends of the columns while the

Bottom PCB connects to the negative ends. In the penetrator, there will be three stacks, adding up to 156 primaries. Each stack will be connected to the other stacks via 18 gauge wires: the Top PCBs will be connected to one another while the Bottom PCBs will be connected to one another. Figure 4.3.9 illustrates the wiring for a stack of batteries. Note that the figure only shows 3 of the 13 columns.

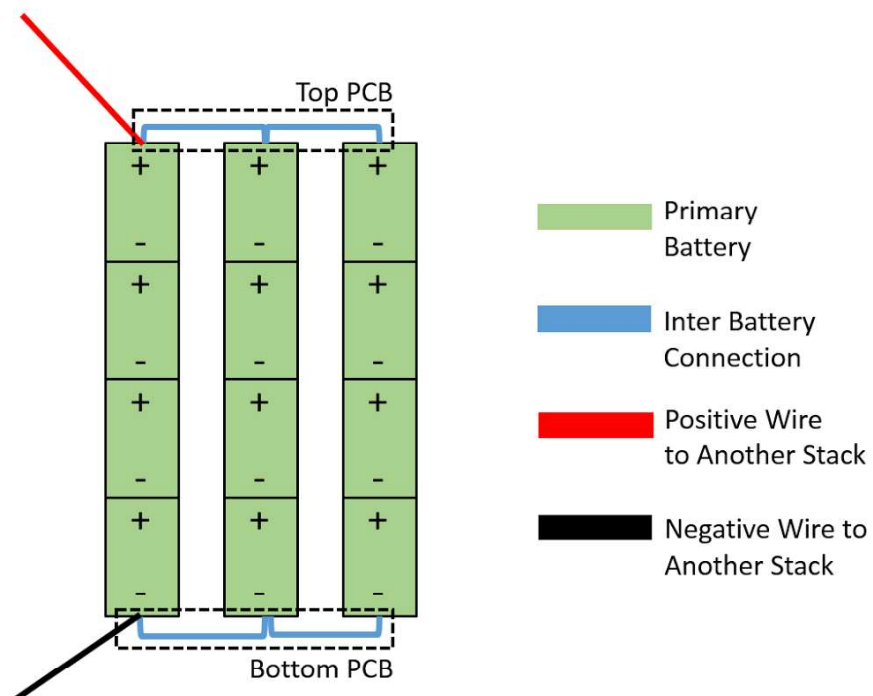


Figure 4.3.9 Primaries Wiring Schematic for One Stack [LY]

The final PCB design is 6" in diameter. There are 0.5" diameter metal pours connected by 20 mil traces. As shown in magenta in Figure 4.3.10, there are D-shaped cutouts for wires to pass through and screw hole cutouts for screws to attach the PCB's to the primary batteries mold. These screws also help compress the batteries together to ensure proper connections. Also, there are two smaller, circular metal pours that allow for wires to be soldered to the PCB. As shown in Figure 4.3.11, the final Bottom PCB, which connects to the negative terminals of the batteries, has D-cell sized spring soldered to the 0.5" metal pours. This is to ensure proper connections between the PCBs and the batteries.

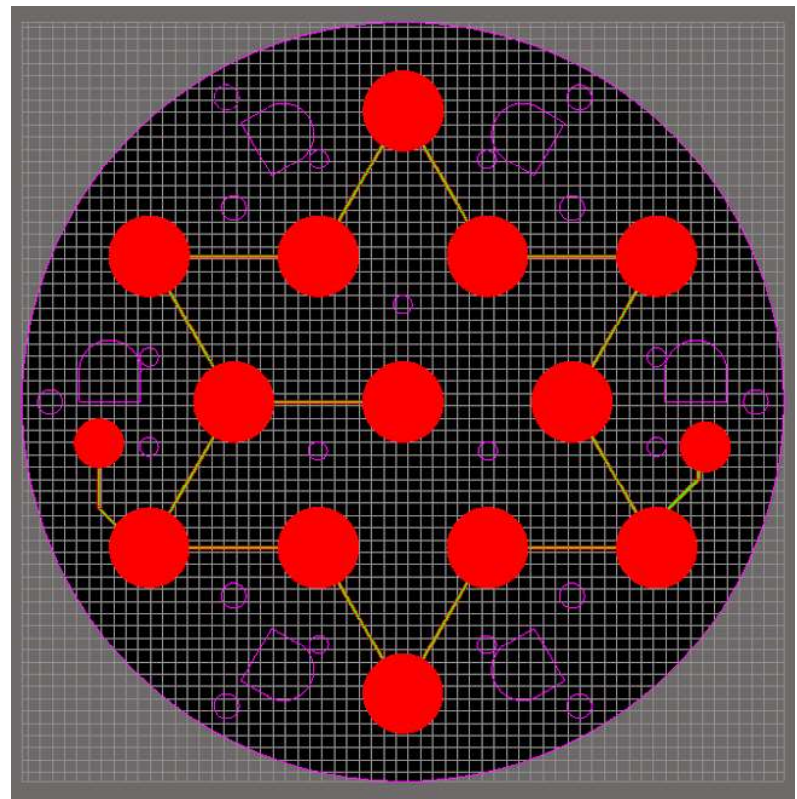


Figure 4.3.10: Primaries Wiring PCB Altium Design [LY]

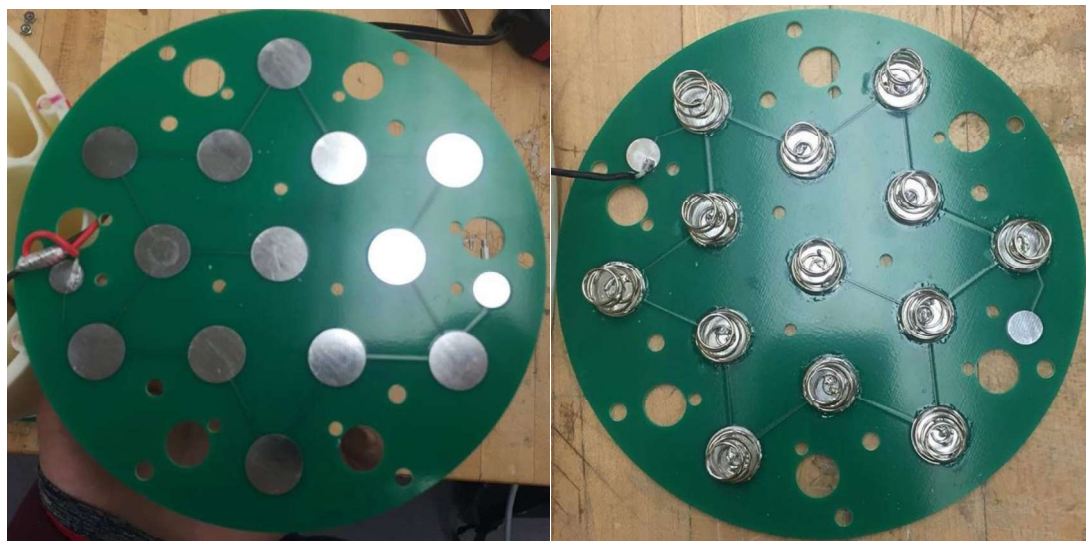


Figure 4.3.11: Final Primaries Wiring PCB Top (left) and Bottom (right) [LY]

4.3.2.3 Secondary Batteries (EL)

In 16.83, Panasonic NCR18650B 3.7V 3400 mAh Rechargeable Lithium Batteries were chosen because a single battery provides at least 3V for 8 days while providing 27.4 mA, the expected current in one battery during the Light Period, in 0°C after being fully charged. To test this, a secondary battery was discharged using a breadboard with a $160\ \Omega$ resistor. The battery was placed inside a freezer. A voltage logger and thermocouple were used to measure the voltage and temperature continuously for the duration of the test. See Appendix I.1 for more details on the test plan. The results are shown below, in Figures 4.3.12 and 4.3.13.

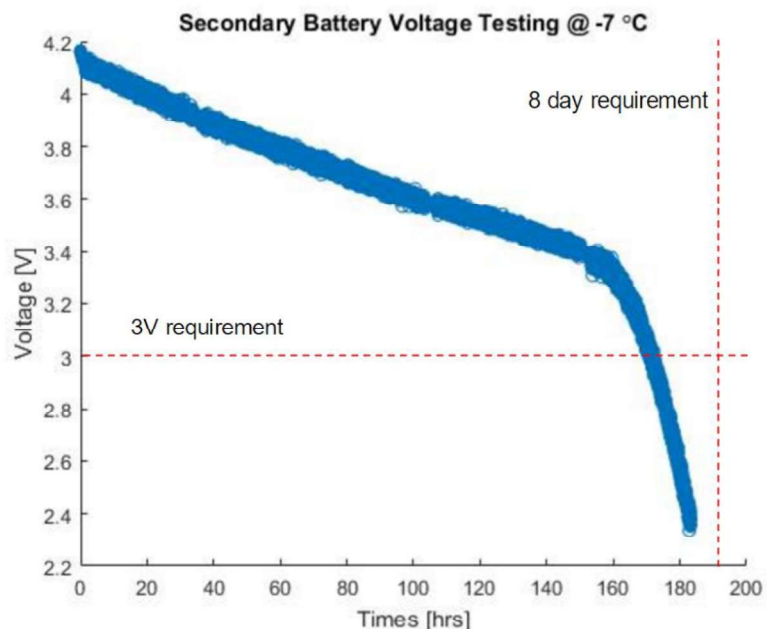


Figure 4.3.12: Secondary Battery Discharge Curve [EL]

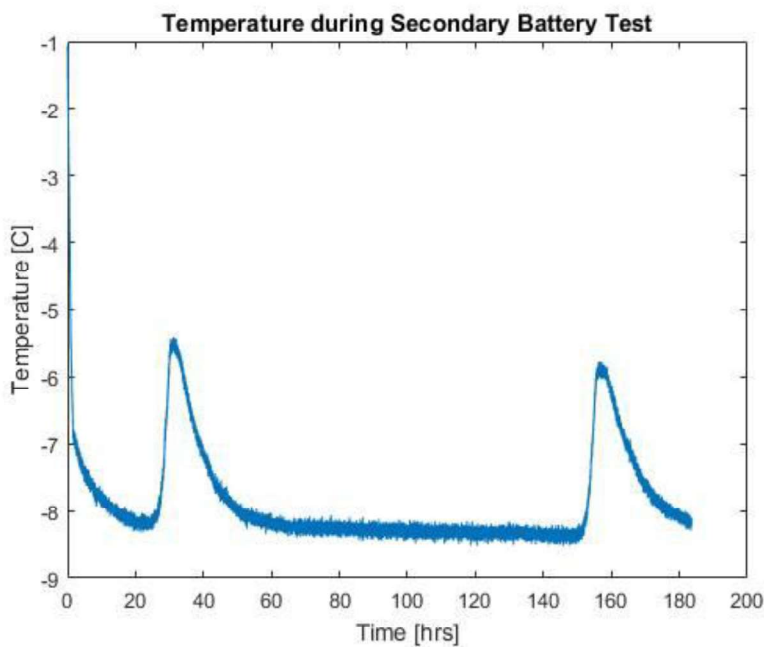


Figure 4.3.13: Secondary Battery Temperature During Discharge [LY]

From the data, it is shown that the battery was able to supply at least 3 volts for 7.15 days. Therefore, the test was unsuccessful. However, due to the freezer's limitations, the average temperature of the battery's environment was -7.4°C. Ideally, the temperature would have been 0°C, so this test will need to be redone. It is expected that if the freezer's temperature is 0°C, the time that it takes a fully charged secondary battery to discharge to 3V will be much closer to 8 days than our result of 7.15 days.

In addition to verifying the discharge characteristics, the batteries should also be tested for cycle degradation and charging characteristics in 0°C.

4.3.2.4 Printed Circuit Boards for Wiring Secondary Batteries (EL and LY)

The secondary batteries are organized to fit in one plane located in the after body of the penetrator. The batteries will be placed in an alternating orientation. There are four batteries to be connected in series, and each set of four needs to be connected in parallel. As demonstrated in Figure 4.3.14, this will result in different wiring for the Top PCB and the Bottom PCB. Finally, there is a positive and a negative wire to connect the entire secondary battery pack to the MPPT.

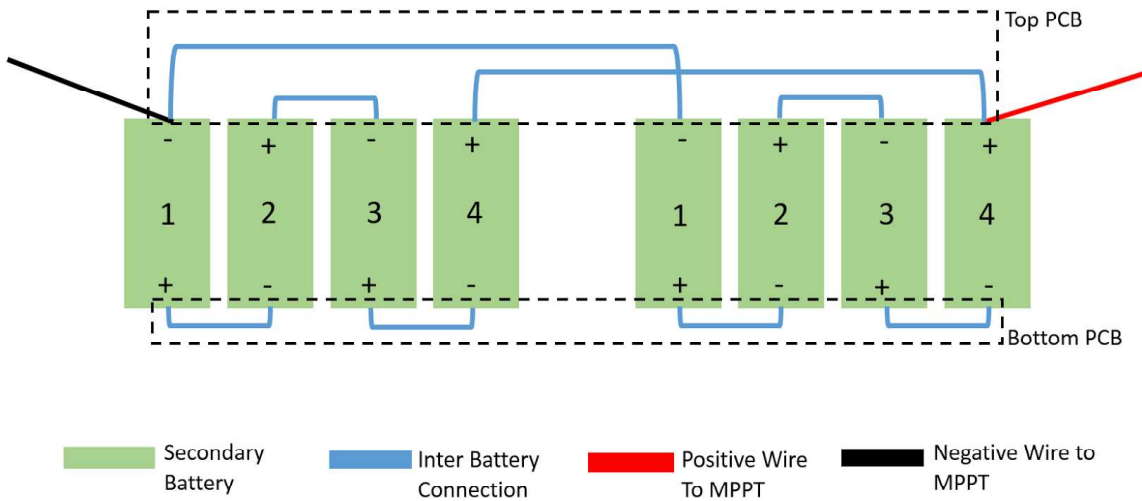


Figure 4.3.14: Secondaries Wiring Schematic [LY]

The final Top and Bottom PCB designs are 14.9" in diameter. Figures 4.3.15 and 4.3.16 show the PCB designs for wiring the secondary batteries. As shown in magenta, there is a 5.45" X 7.65" rectangular cutout for the avionics stack to pass through and holes for standoffs and screws to help compress the batteries together. The circular pours (red circles) allow AA-cell sized springs to connect to the batteries' negative terminal, and the square-shaped pours (red squares) allow AA-cell sized, dimple-shaped contacts to connect to the batteries' positive terminal. (It should be noted that the secondary batteries, and not the primary batteries, require positive contacts because their outer, plastic covering prevents a proper connection.) The pours are connected with 20 mil traces. Figures 4.3.17 shows the final PCBs with all of the contacts soldered to the metal pours. There are two, 18 gauge wires soldered to the Top PCB to connect the secondary batteries to the MPPT.

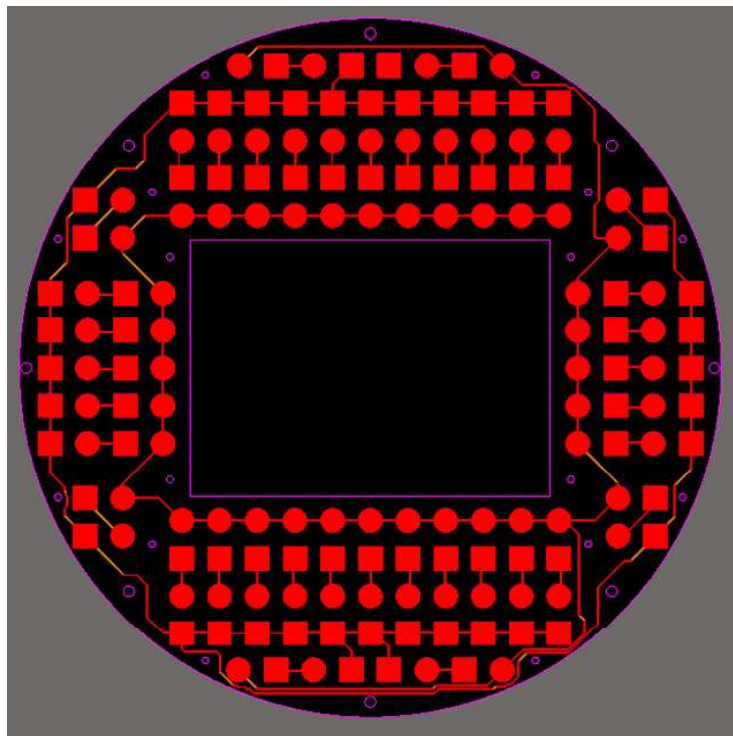


Figure 4.3.15: Top Secondaries Wiring PCB Design

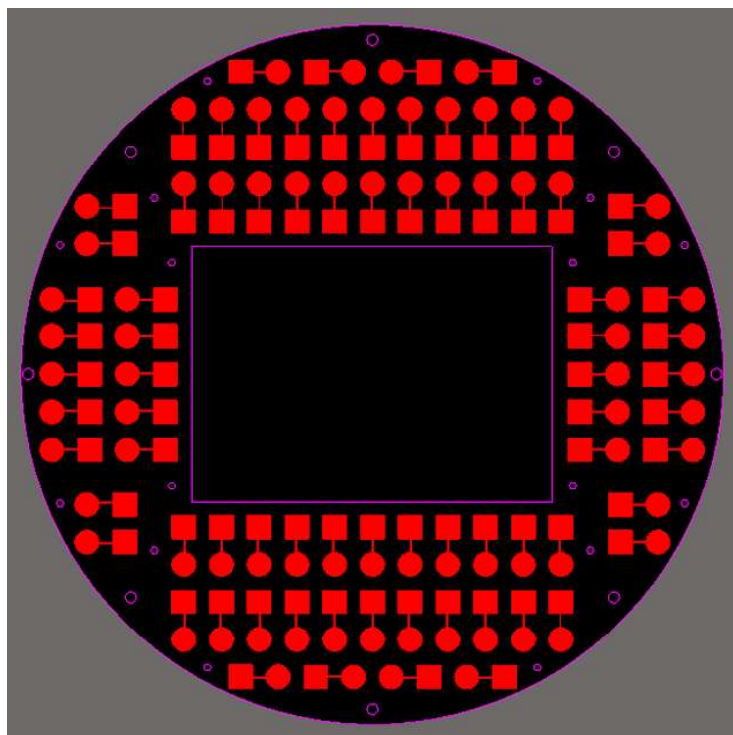


Figure 4.3.16: Bottom Secondaries Wiring PCB Design

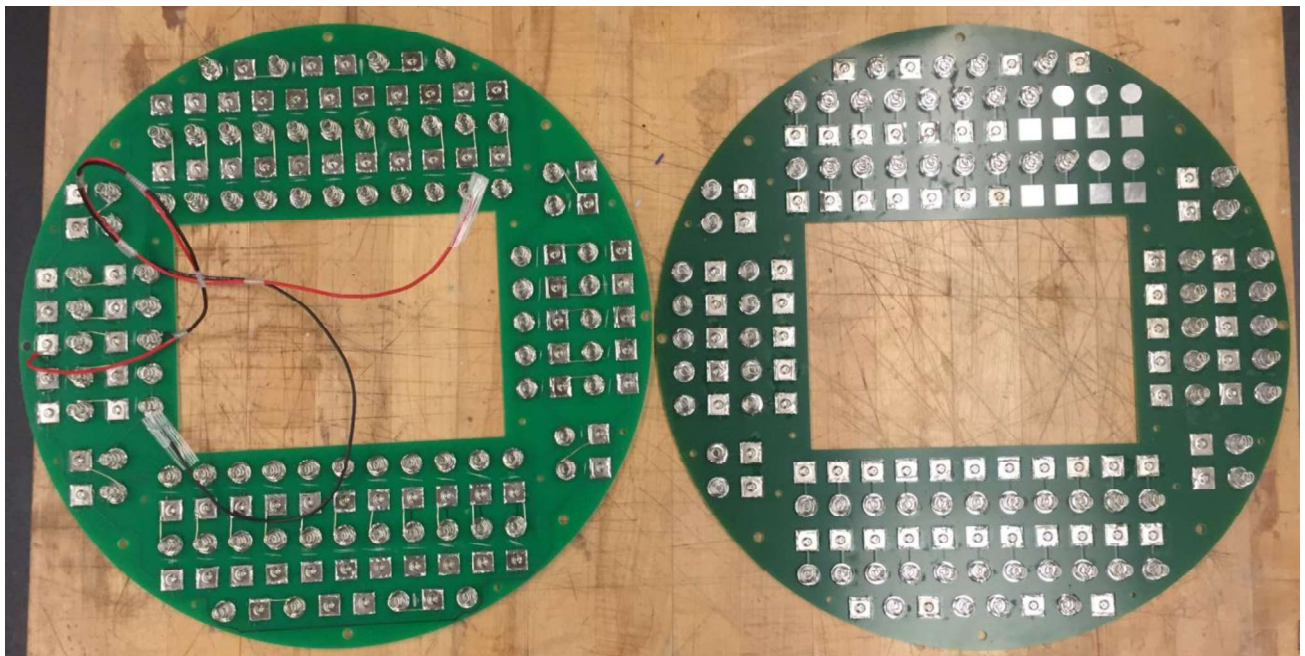


Figure 4.3.17: Final Secondaries Wiring PCB Top (Left) and Bottom (Right) [LY]

4.3.2.5 Primaries and Secondaries Internal Resistance Testing (LY and EL)

Although not a requirement for acceptance of the primaries or the secondaries, one useful piece of information is the internal resistance of the batteries to estimate the amount of heat they will produce to help the future thermodynamics team better predict the penetrator's internal temperatures. The primaries internal resistance test consisted of four primary batteries connected in series, and the total voltage was measured. Then, the batteries were discharged using an 1100 ohms resistor to simulate the load during the Dark Period that a pack of four batteries would experience. The voltage was measured again. Using the difference in voltage and the current, the internal resistance was calculated to be 25.37 ohms for four batteries in series. This is equal to a power dissipation of 172 mW for all 156 primaries. Refer to Appendix I.1 for a detailed test plan.

A similar test was done with the secondaries. A 600 ohms resistor was used to simulate the load during the Light Period that a pack of four secondary batteries would experience. The internal resistance was calculated to be 0.7227 ohms for four batteries in series. This is equal a power dissipation of 20 mW for all 148 secondary batteries. Refer to Appendix I.1 for more on the test plan.

4.3.2.6 Prototype Solar Panels (FT)

Solar panels are the main power source throughout the light period of the mission. As seen in the figure underneath, the solar panels subpart consist of a total of 6 solar panels, of which each has 8 solar cells. This arrangement was designed in order to bring up the voltage to order of magnitude 20V in order to power the MPPT, which necessarily requires more voltage than it outputs.

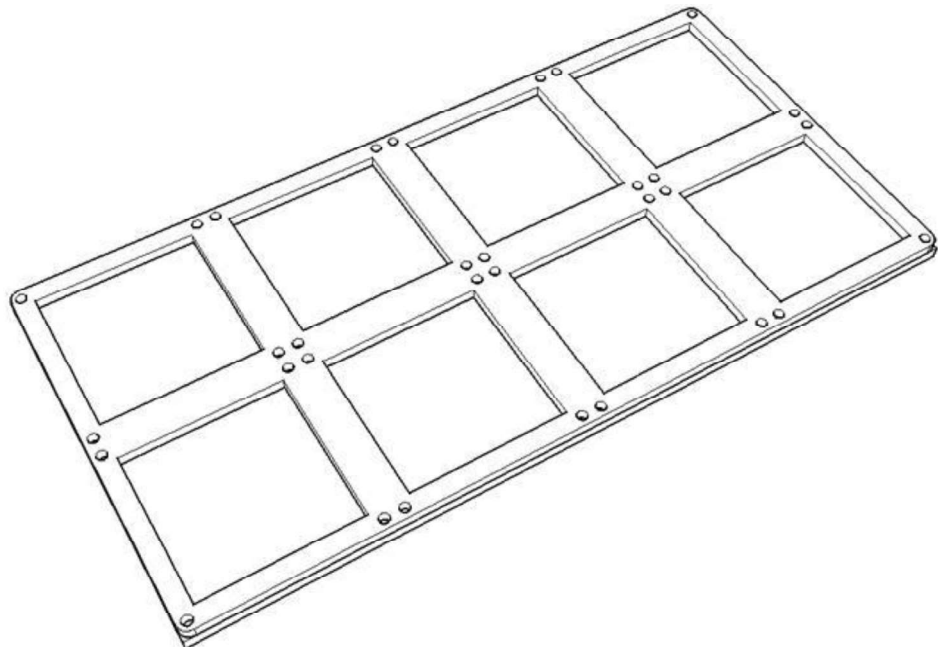


Figure 4.3.18: Laminated Solar Panel [JV]

In the testing period we tested the solar panels power output in various conditions, including limited lighting, regular lighting, as well as varying temperature of the solar panels. Varying lighting was naturally easy to provide, as we were very weather-dependent. Varying internal temperature of the solar panels was a little more complicated as it required us to put in the solar panels into a freezer until they reached equilibrium temperature of about 0 degrees Celsius.



Figure 4.3.19: Solar Panels Array [FT]

The test results under standard lighting and temperature were promising. The solar panels provided us with a power output of 2.5 W per panel, ultimately providing a total of 15 W from the array of solar panels. While this result is significantly lower than what we would expect from triple junction solar panels, they provide a sufficient amount of power to ensure that we are not discharging the secondary batteries in the sun even when we are under the highest power draw of ~14 W.

The results under lower temperature were much less promising, as the power output dropped almost 5 fold. This, however, was to be predicted as the cheap single-junction solar panels were not rated for any significant temperature drops.

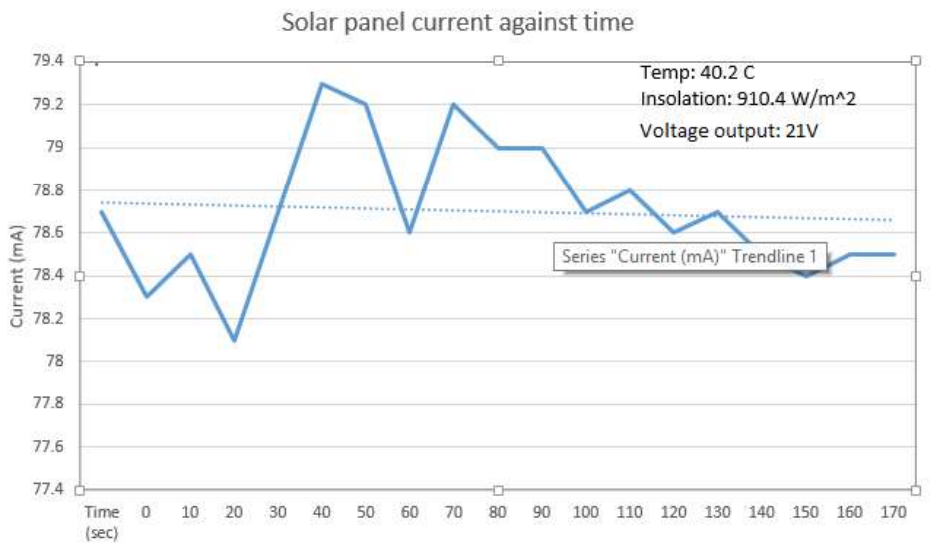


Figure 4.3.20: Worst Solar Panel Current Output at Standard Insolation and Temperature [FT]

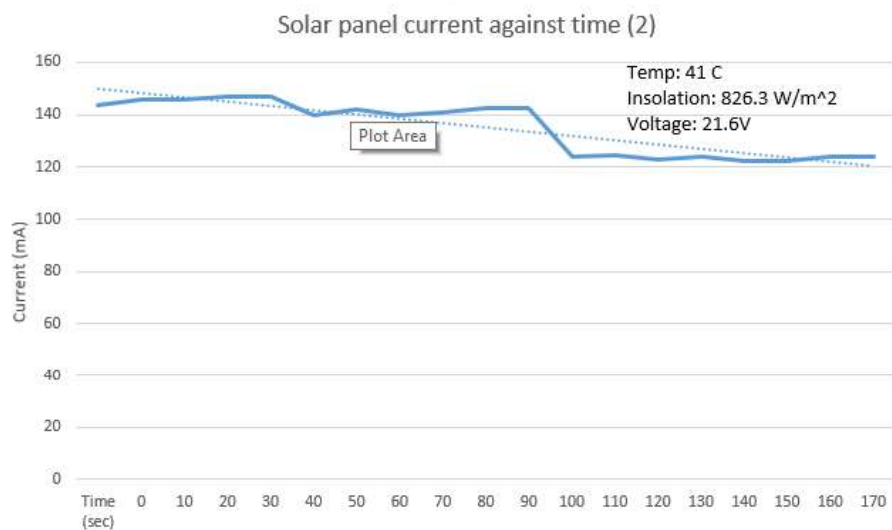


Figure 4.3.21: Average Solar Panel Current Output at Standard Insolation and Temperature [FT]

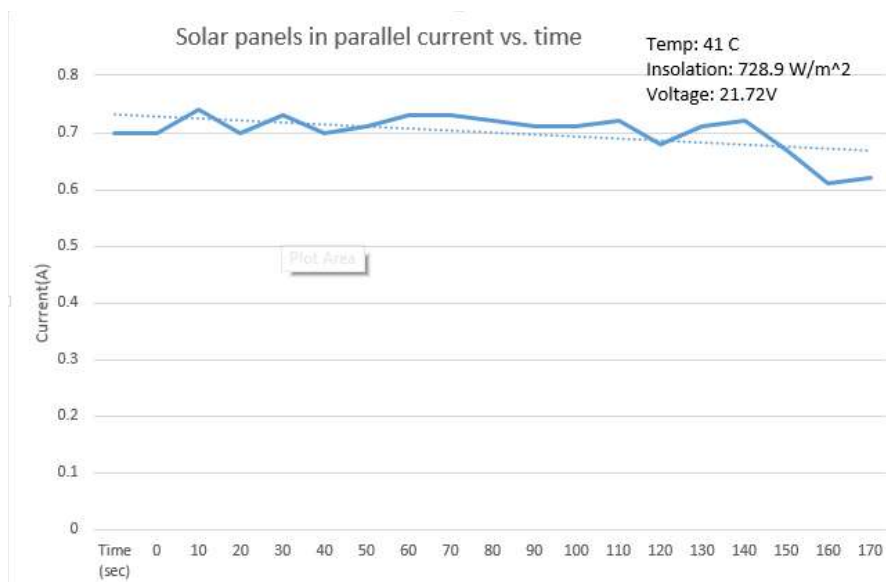


Figure 4.3.22: Solar Panels Array Current Output at Standard Insolation and Temperature [FT]

4.3.2.7 Mission Model Solar Panels (FT)

During the class, we also had the opportunity to test extremely high efficiency triple-junction solar cells produced by Spectrolab. The Improved Triple Junction solar cells, which we test, came in a CIC form (Solar Cell, Interconnect + Glass), which greatly simplifies the assembly process, as we do not have to worry about hooking up the silicone to the interconnects or bypass diode.

The solar cells were predicted to have peak efficiency of 26.8%, which is significantly higher than what we measured in the single junction cells. We ended up obtaining the peak efficiency of 21% at 919 W/m², which corresponds to the recommendable voltage and current values for the solar cells. Note that efficiency is calculated with the following equation:

$$\eta = \frac{V_{OC} I_{SC} FF}{S A_{cells}}$$

where η is the efficiency, V_{OC} is the open circuit voltage, I_{SC} is the short circuit current, FF is the fill-factor, which we assume to be 0.7, S is the insolation and A_{cells} is the total area of the cells.

Refer to Figure 4.3.23 to observe the power output plot of the cells.

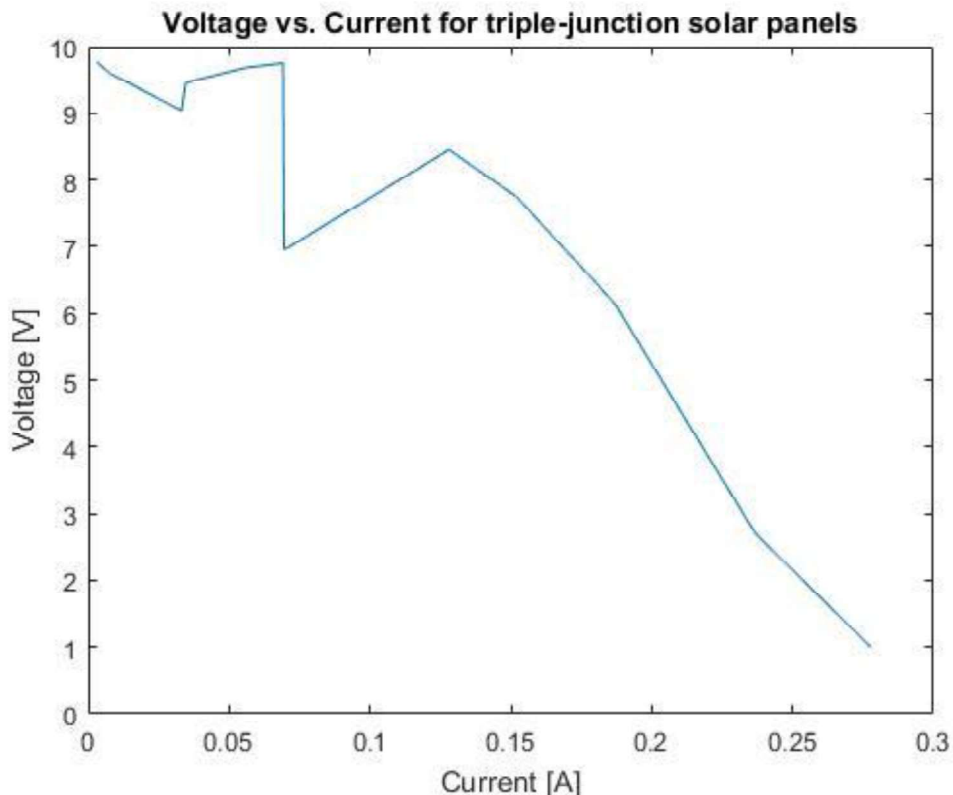


Figure 4.3.23: Power Outputted by Triple-Junction Solar Panels. [FT]

The slightly lower efficiency of 21% is not problematic since the simulation in 16.83 assumed 20% efficient solar panels.

Contributions: In testing the expensive solar panels, we have determined that they are fit for mission use and adhere to the model used in 16.83.

4.3.2.8 Maximum Power Point Tracker (MPPT)(JV)

The MPPT used in the prototype is an OTS SunSaver MPPT Solar Controller and was chosen because it was available for free use in the SSL. The MPPT was not tested individually because it requires input from solar panels and secondary batteries. Refer to section 4.3.3.1 for more details on this test.

For the mission, we suggest using Genasun GV-10 12V 140W because it has higher peak efficiency (98.3% over 93%) and is specified to work under the expected temperatures. Additionally, at \$109, it is relatively low cost. A tabular comparison of the two MPPTs can be found in Table 4.3.3.

Table 4.3.3: Prototype and Mission Model MPPT Comparison [JV]

SunSaver MPPT	Genesun MPPT
Prototyping	Mission
No Cost	\$109
-40 to 60 operational range	Adequate operational range
93% peak efficiency	98.3% peak efficiency
Protects batteries from overcharging	Low self-consumption 0.09A

The efficiency specified on the MPPTs is not clear; it is not obvious if the efficiency includes ‘losses’ due to self-power draw or if the efficiency pertains only to losses in channeling solar power input to batteries. The night self-consumption of the MPPT was one of the criteria of the choice in the design process, and as such was the lowest we could find at 0.9mA at nominal 14.4V.

Secondly, only peak efficiency is specified exactly. The efficiency is supposed to fluctuate between 96-98% on average as described by the producer, although the exact efficiency under Antarctic conditions should be tested in the future.

Contributions: We have determined that an OTS MPPT functions as specified without much trouble.

4.3.2.9 Switching Circuit [JV]

The switching circuit had to be completely redesigned because, unfortunately, the design proposed in 16.83 was fatally flawed. After many, many iterations, circuit board alterations, breadboarding, component testing, language learning, and long nights, the following circuit is functional and has high power efficiency.

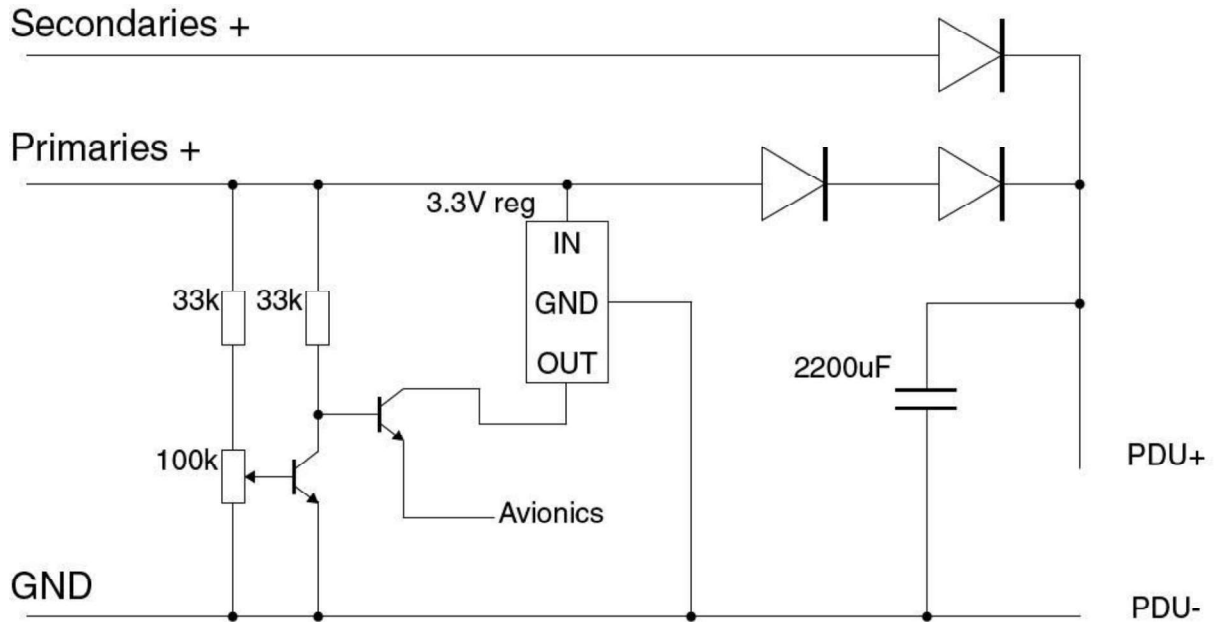


Figure 4.3.24: Circuit Diagram of switching circuit [JV]

The main power draw of the switching circuit comes from the Schottky diodes used. There are two diodes used on the primary connections in order to induce a voltage drop before they go out to the PDU. This voltage drop ensures that the secondary batteries are drawn from while they have healthy voltage level; only when the secondaries fall to low voltage are the primaries used.

The voltage indicator circuit uses two MOSFETs; the first one takes an input from the potentiometer which will output high with voltage of 14.4V under normal conditions, saturating the first MOSFET. If primary voltage falls low the first MOSFET is no longer saturated, sending a high voltage into the second one. The second part effectively acts as a MOSFET activated not gate to give a high to avionics when primary voltage falls low. The capacitor is for smoothing and to provide buffer during diode switches. During expected power draw, a time constant, $\tau = RC$, is expected to be over 30ms given the effective resistance of the penetrator. This is greater than switching speed of the diodes used in prototyping and also of the recommended mission diodes. If this does pose a problem during high power draws, a larger capacitor can be used.

The switching circuit was tested for efficiency under 3 load types: peak, minimum, and average. Efficiency was calculated as: [power to load]/[total power to circuit]

Table 4.3.4: Table to Show Data for Efficiency Calculations [JV]

Load (W)	Point in circuit	Voltage (v)	Current (Amps)	Efficiency (%)
15	Secondary batteries to circuit	14.4	0.139	
15	Primary batteries to circuit	14.4	0.006	
15	Circuit to load	13.8	0.139	91.8
4	Secondary batteries to circuit	14.4	0.259	
4	Primary batteries to circuit	14.3	0.006	
4	Circuit to load	13.8	0.256	92.8
2	Secondary batteries to circuit	14.4	0.932	
2	Primary batteries to circuit	14.4	0.091	
2	Circuit to load	13.8	0.932	87.3

The switching circuit has minimum efficiency of 87.3% with the diodes used in the prototype, which is not quite within the 30% buffer allocated for distribution losses in 16.83 (that includes 90% efficient PDU and 93% efficient MPPT). However, this can be amended with the use of diodes with a lower voltage drop.

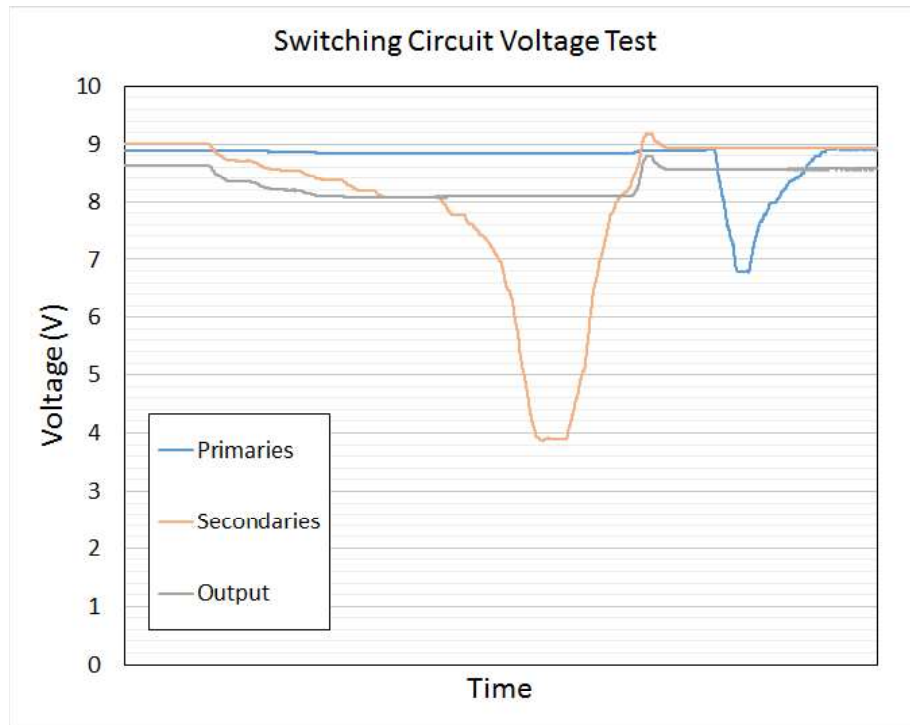


Figure 4.3.25: Input Voltages and Output Voltage of Switching Circuit [JV]

The voltage logger took up to only 10V; thus we set a target voltage of 9V. As shown in Figure 4.3.25, the output to the PDU from the switching circuit is within 1V of the target voltage as one of the input voltages falls. We also see that there is no power outage between switching of power supplies.

Contributions: a circuit that is within cost, weight and volume which is able to interface between primary and secondary power sources and favor the secondary power supply as necessary.

The switching circuit is also capable of sending a signal during an emergency. As shown in Table 4.3.5, a signal is sent to avionics at 3.3V if the primary batteries output below 12.5V, indicating that the primary pack is running out of power.

Table 4.3.5: Output to Avionics [JV]

Primary Vin	Vout to Avionics
14.4V	0.12V
12.5V	3.29V

10V	3.29V
-----	-------

Contributions: Method of indicating critical power loss and sending the signal to the appropriate subsystem

The switching circuit prototype is currently on a breadboard. A PCB has been planned but was not ordered for 16.831 due to time constraints. Figure 4.3.26 depicts the new PCB design for the switching circuit.

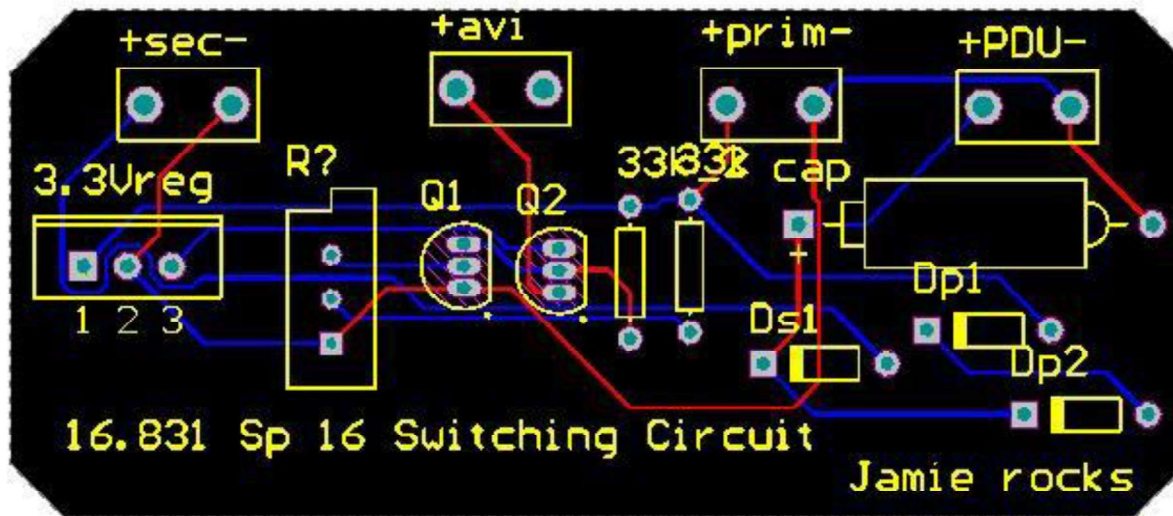


Figure 4.3.26: Proposed 2-Layer PCB for Switching Circuit. [JV]

Lastly, the switching circuit has potential to attain higher efficiency with the use of diode with a smaller voltage drop; the diodes used in the prototype had a voltage drop of about 0.5V at peak draw and therefore sucked up a significant amount of power. Lower voltage drop diodes are cheaply available and would improve performance.

4.3.2.10. Power Distribution Unit (PDU) (CT)

The power distribution unit (PDU) provides power to various hardware components in the system at the necessary voltages. As seen in the block diagram in Figure 4.3.1, the PDU receives power directly from the switching circuit, and then distributes this power to the rest of the system. Also evident in Figure 4.3.1 are the specific hardware components to which the PDU distributes power, and the voltages that they need in order to operate properly. Figure 4.3.27 provides more detail, including the specific voltage regulators used and the subsystems to which the hardware components belong.

The PDU provides voltages from a single 14.4 V bus voltage source. A single power bus is implemented in the interest of simplicity and minimizing risk. Two switching voltage regulators are then used to step-down the bus voltage to operating voltages of 12.0 V and 5.0 V. The 5.0 V is also stepped down to 3.3 V by a linear voltage regulator to provide an additional power output of 3.3 V. Thus, the PDU provides operating voltages of 12.0 V, 5.0 V, and 3.3 V to the system. Switching voltage regulators were selected in the case where a large amount of power would be converted, and thus losses would be significant had a linear regulator been used. A linear voltage regulator was selected to step down the voltage from 5.0 V to 3.3 V because only a small amount of power (about 134 mW) is required by the hardware components receiving 3.3 V. Thus, a switching voltage regulator would not significantly increase the overall efficiency of the PDU, especially not at the cost of a higher price and more complicated voltage regulator.

The Linear Technology LTC 3129 buck-boost DC/DC converter was chosen to provide the 12.0 V operating voltage. This regulator has an input voltage (V_{in}) range of 2.42 V to 15 V, an output operating range of 1.4 V to 15.45 V, and is functional up to a current draw of 200mA. It has an efficiency of 90% under expected operating conditions (V_{in} of 14.4 V, V_{out} of 12.0 V, and a current draw of 22mA), and shall continuously power the Trillium-Compact Seismometer. Since the sensors subsystem team was unable to obtain this seismometer, we were unable to test this integration. However, testing of the PDU demonstrated that the voltage regulator operates as expected, providing a V_{out} of 11.94 V, given a V_{in} of 14.4 V, and under a current draw of 21mA.

The Linear Technology LTC 3649 synchronous monolithic step-down regulator was chosen to provide the 5.0 V operating voltage. This regulator has a V_{in} range of 3.1 V to 60 V, an output operating range of 0.0 V to (V_{in} - 0.5 V), and is functional up to a current draw of 4A. It has an efficiency of about 92% under expected operating conditions (V_{in} of 14.4 V, V_{out} of 5.0 V, and a current draw 250mA to 830mA), and shall continuously power both the transceiver and GPS antenna. Testing of the PDU demonstrated that the voltage regulator operates as expected, providing a V_{out} of 4.98 V, given a V_{in} of 14.4 V and a current draw of 250mA, and a V_{out} of 4.93 V, given a V_{in} of 14.4 V and a current draw of 960mA. Integration testing also confirmed that the PDU could provide the necessary power to both the transceiver and GPS antenna under the full range of current draws expected.

The Linear Technology LT 1762 micro power, low noise, low dropout regulator was chosen to provide the 3.3 V operating voltage. This regulator has an input voltage (V_{in}) range of 1.8 V to 20 V, a fixed output voltage of 3.3 V, and is functional up to a current draw of 150mA. It has an efficiency of 66% under expected operating conditions (V_{in} of 5.0 V and V_{out} of 3.3V), and shall continuously power the PSoC, memory card, Avionics' current sensors, and the tilt/impact sensor. Testing of the PDU demonstrated that the voltage regulator operates as expected, providing a V_{out} of 3.29 V under a current draw of 40mA. Integration testing also confirmed that the PDU could provide the necessary power to these four hardware components simultaneously.

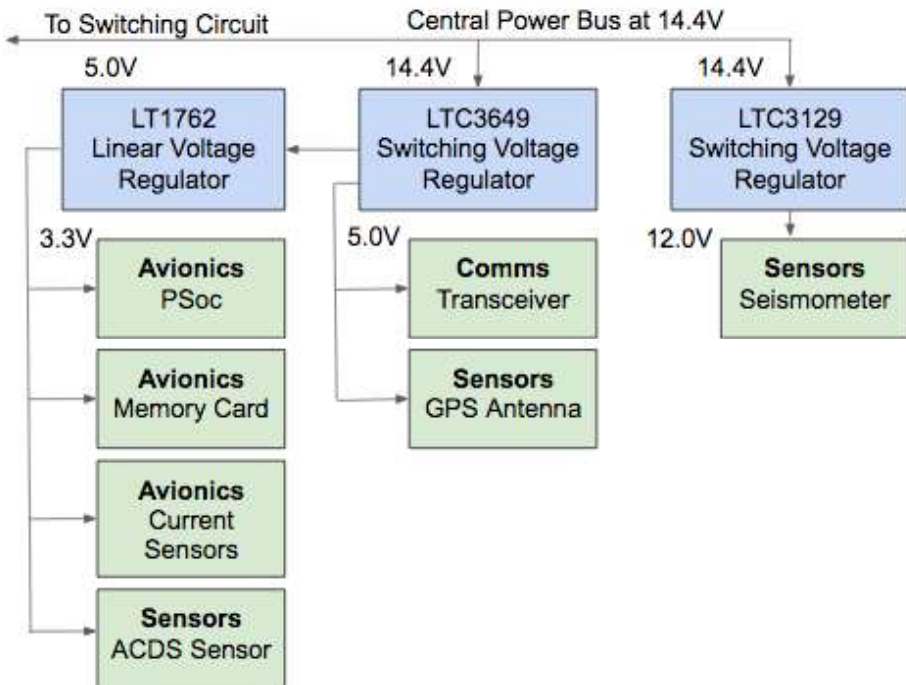


Figure 4.3.27: [CT] - Diagram of System Components and Bus Voltages Received and Used

The top line in Figure 4.3.27 represents the central power bus coming from the switching circuit. The blue boxes represent each of the voltage regulators selected. The switching voltage regulators take their input voltage directly from the central power bus, and the linear voltage regulator takes its input voltage directly from the LTC 3649 regulator. The green boxes represent each of the power-drawing hardware components that need the specified voltage on the bottom of each blue box.

The PDU circuit board itself, see Figure 4.3.28 below, was designed to fit in the penetrator and easily connect with the hardware components to which it provides power. It is a 2-layer PCB, and its dimensions are 4 inches long by 6 inches wide. There are four mounting screw holes at the corners, spaced 0.25 inches from each side, designed for size 2-56 screws. The traces to the LTC 3649 regulator, and from the LTC 3649 regulator to the 5.0 V output, are necessarily large (at least 108 mils) to accommodate a current of up to 3A. The transceiver may attempt to pull this much current. The other traces do not require a large width and are 10 mils wide.

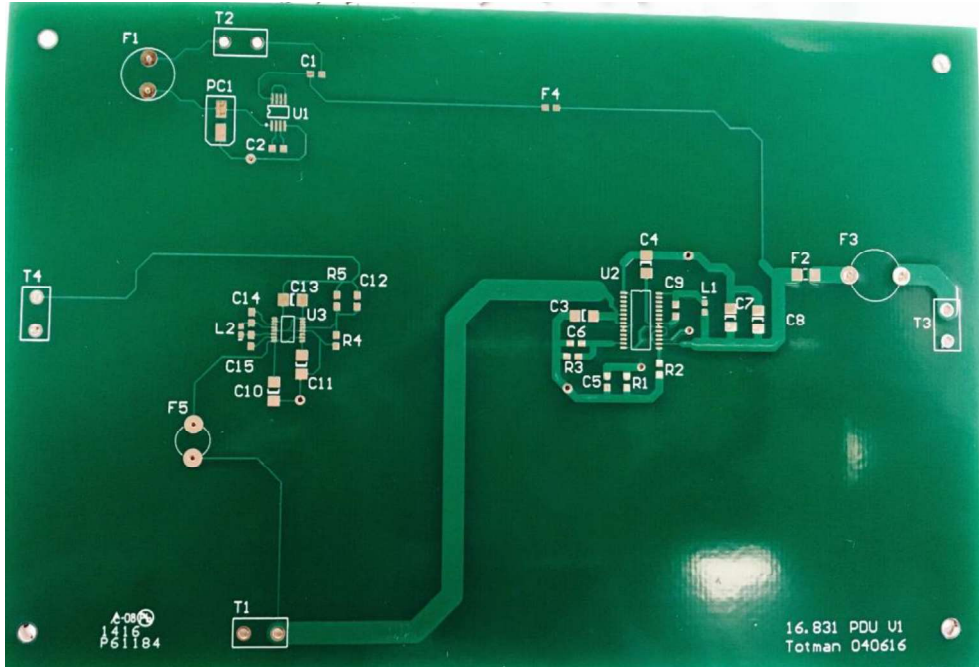


Figure 4.3.28: [CT] - PCB Layout of the PDU

Many issues with the PDU's circuit board design were detected during testing, and thus there are several recommended modifications to the current design. See Figure 4.3.29 below for the recommended PCB layout of a new version of the PDU. One modification in this design is the removal of F3, the high current limiter, as fuse F2, a PTC resettable fuse with a hold current of 1.5A, is more than sufficient to prevent a high current from damaging the transceiver. Other modifications include replacing fuses F1 and F4, both PTC resettable fuses, with PTC resettable fuses with higher hold currents, 200mA and 150mA respectively. During testing, inductor L1 needed to be replaced with an inductor with a higher current limit, 2.8A compared to 90mA, so this change is reflected in the new board layout. The footprint for PC1 needed to be turned in the opposite direction, and pins 1 and 2 on U1, the LT 1762 voltage regulator, were connected with a trace.

The most important modification, however, is the addition of heat sinks, or "power planes," for three groups of pins on U2, the LTC 3649 voltage regulator. These groups of pins are the Vin pins, the PGND pins, and SW pins. In testing, external heat sinks in the form of thin, bendable pieces of copper needed to be soldered perpendicular to the PDU circuit board in order for the PDU to function properly. These heat sinks were added to the top layer of the PCB layout.

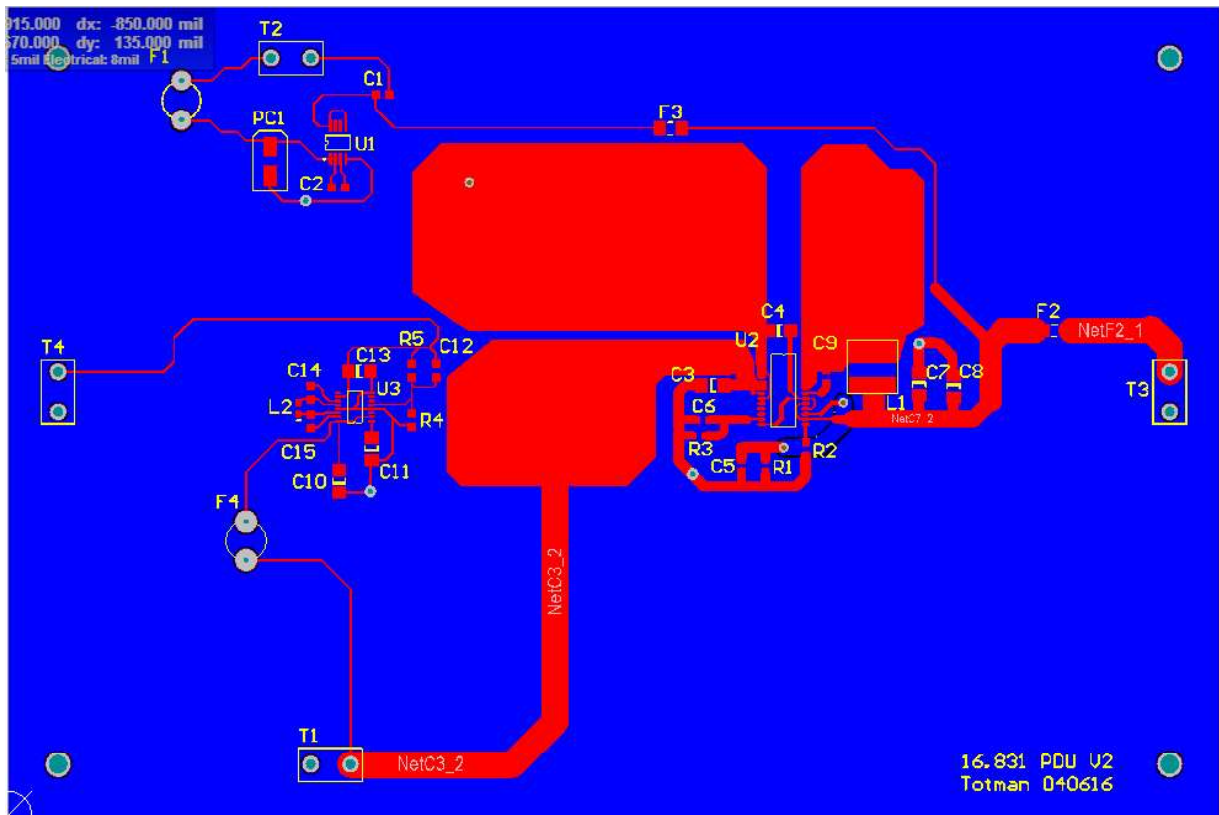


Figure 4.3.29: [CT] - PCB Layout of the Recommended PDU

4.3.3. Subsystem Integrated Testing

4.3.3.1 Solar Panels, Secondaries, and MPPT (FT)

Solar panels, secondaries, and MPPT integrated testing was done to ensure that the behavior of the MPPT was as described by the producer. As such we first connected the load of 270 ohms to the MPPT, then connected 4 partially charged secondary batteries, and finally, connected the array of six solar panels.

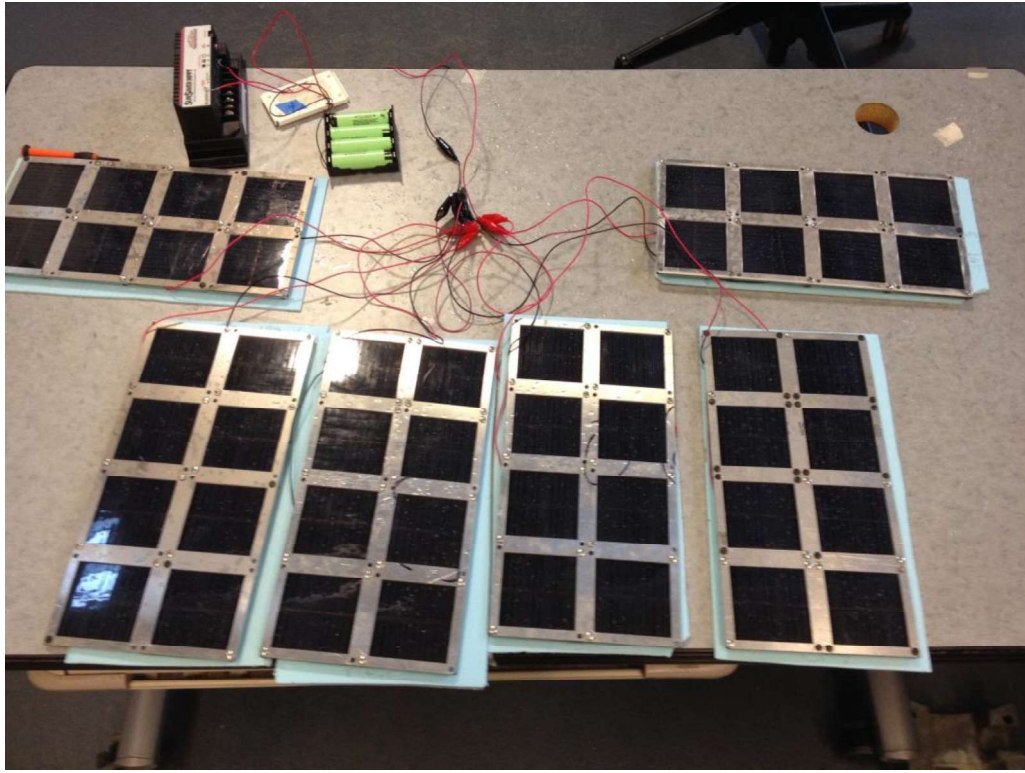


Figure 4.3.30: Solar panels, MPPT and Secondary Batteries Testing Setup

Irrespective of the insolation, the MPPT outputted the expected voltage and current throughout the entire test. This confirmed the design of any MPPT, which essentially first charges the batteries, and then outputs the power. This implies that, at any point, we should be expecting a steady voltage and current output depending specifically on how charged the secondary batteries are at that specific moment.

4.3.3.2 Switching Circuit and PDU (JV, FT)

Two variable power sources simulating primary and secondary batteries were put into the switching circuit at 14.4V. This allowed us to quickly simulate discharging of the batteries. We then connected the PDU to the switching circuit, and tested the outputs specified to be at 3.3V for Avionics and 5V to Comms and Sensors.

We then proceeded to test those at the expected loads throughout the mission, as Avionics required 0.134W (which corresponded to a load of 83 Ohms), and Comms power intake was at 4.4W (which corresponded to 6 Ohms). The tests confirmed that we are capable of providing the necessary power irrespectively of the relative charge on the secondary and primary batteries. In particular, we could observe a steady output at the required powers at the required voltages.

4.3.4 System Integrated Testing (LY and EL)

Once the switching circuit, PDU, and primary batteries had been tested, the Power subsystem began to integrate with other subsystems' electronics. Table 4.3.6 shows the results of our preliminary tests. Twelve batteries were used and placed inside the primary battery stack, which was connected to the switching circuit. The switching circuit was connected to the PDU which was the main interface to the other subsystems' electronics. The starting voltage remained constant, approximately 14.67 V. As the current being pulled increased, the voltage into the switching circuit decreased. This trend was to be expected since this is typical behavior of batteries. If more batteries are added in parallel, the current being pulled from the batteries will decrease. Therefore, in the future, to test the seismometer, which requires 12V, at least 24 batteries are needed.

As shown in the table, there is a voltage drop across the switching circuit; this was expected since the diodes used in the switching circuit prototype were not very efficient. From the switching circuit, the power was properly distributed through the PDU. The voltage was dropped to the necessary voltages (3.3V for Avionics and 5V for the GPS and Communications), and the other subsystems' verified that their components were being powered. From this test, it has been demonstrated that the penetrator's instruments, except the seismometer, can be powered successfully through our subsystem.

Table 4.3.6: Table to Show Results of Integrated Testing [LY]

Batteries Starting Voltage (V)	Vin Switching Circuit (V)	Vin PDU (V)	Vin Avionics Integration Board (V)	Vin GPS (V)	Vin Comms Standby (V)	Vin Comms During Call (V)	Other Subsystems' Verification
14.67	14.47	13.78	3.3	---	---	---	Yes
14.67	13.62	13.02	---	4.98	---	---	Yes
14.66	13.04	12.26	---	---	4.97	---	Yes
14.67	10.89	10.55	---	---	---	4.96	Yes
**	**	**	---	4.97	---	4.97	Yes

** Did not measure --- Component not connected

4.3.4 Power conclusion (LY)

Individual components of the power system have room for further design refinement, which has been discussed in their respective sections. No major design changes have been identified so far. However, it is important to note that both low temperature and drop testing still need to be performed on most of the subsystem. Other than the Dark Period, it is still unclear whether the penetrator can be powered sufficiently.